



Ablation resistance of C/C-SiCO nanoporous ceramic composites with TaSi₂-MoSi₂-ZrB₂-borosilicate glass coating

Xiafei Li^{1,2}, Junzong Feng², Xingyu Wu¹, Jin Jiang^{1,*}

¹Aerospace Technology Institute, China Aerodynamics Research and Development Center, Mianyang, Sichuan 621000, China

²Science and Technology on Advanced Ceramic Fibers and Composites Laboratory, College of Aerospace Science and Engineering, National University of Defense Technology, Changsha, Hunan 410073, China

Received 15 August 2023; Received in revised form 15 November 2023; Accepted 29 November 2023

Abstract

The development of high-speed aerial vehicles urgently requires high-performance integrated materials for ablation resistance, thermal insulation and oxidant protection under high temperature. The previously prepared carbon aerogel composites (C/CA), with ultra-high temperature thermal insulation properties, were impregnated with SiCO precursor sol and pyrolysed in nitrogen atmosphere at 1200 °C. The impregnation/pyrolysis process was performed once, twice and thrice to obtain three different C/C-SiCO nanoporous ceramic composites. Further, TaSi₂-MoSi₂-borosilicate glass (TM-BG) coating or TaSi₂-MoSi₂-ZrB₂-borosilicate glass (TMZ-BG) coating was prepared on the surface of the C/C-SiCO through slurry brushing combined with graphite powder embedded sintering process. By simulating the actual application environment through oxygen acetylene flame ablation test, the ablation resistance of the samples was studied and their oxidation mechanism was analysed. The results show that the ablation rate of the C/C-SiCO after 200 s ablation at 1600 °C decreases with the increase of the number of impregnation/pyrolysis steps and that the ablation resistance of the coating modified C/C-SiCO was significantly enhanced. The addition of ZrB₂ to the coating improves the compatibility between the substrates and the coating, and the TMZ-BG coated sample has better ablation resistance. At high temperature, the borosilicate glass in the coating is in a viscous flow state. Meanwhile the SiO₂ generated by the oxidation of other silicide raw materials forms a dense glass layer on the coating surface, which can be used as an oxygen barrier to provide better protection for the substrates. The coating-modified C/C-SiCO porous ceramic composites are expected to be used as a high-temperature ablation-resistant material for the thermal protection system of new aerospace vehicles.

Keywords: C/C-SiCO porous ceramics, silicide coating, high-temperature stability, ablation resistance

I. Introduction

With the continuous increase in flight speed and extended flight time of high-speed aerial vehicles, the accumulation of aerodynamic heating on some key parts of the aircraft windward surface is extremely serious [1]. The harsh thermal environment has put forward an urgent demand for integrated materials for ablation resistance, thermal insulation and high-temperature resistance. With the application of aircraft nose cones and wing leading edges as the background, the Ames Re-

search Center of NASA developed a TUFROC (toughened uni-piece fibre reinforced oxidation-resistant composite) composed of a heat resistant cap coated with gradient coating on the surface and an internal insulation substrate [2]. At present, it has been successfully applied to the high-speed aircraft X-37B demonstration aircraft. Among them, the substrate of the heat resistant cap is chopped carbon fibre reinforced SiCO ceramic composites and the surface is coated with MoSi₂-TaSi₂-SiO₂ high emissivity coating. The integrated material still has good thermal shock resistance and thermal radiation at above 1650 °C, and shows good ablation resistance in 300 W/cm² heat flow.

Compared to dense ceramics, SiCO nanoporous ce-

* Corresponding author: tel: +86 2465624,
e-mail: jjjnpu@163.com

amics have lower thermal conductivity [3] and the bond density of Si–C–O endows them with higher network structure strength, thereby achieving good high-temperature stability [4]. The fibre-reinforced SiCO ceramic composites can serve for a long time in the temperature range of 600–1260 °C [5]. Our research group has previously carried out work on carbon fibre reinforced SiCO nanoporous ceramic composites (C/SiCO) [6,7]. The results showed that the thermal conductivity of C/SiCO at room temperature is low, but there is still significant room for improvement in its insulation performance at high temperatures. Considering that carbon aerogel composites (C/CA) can be used at temperatures up to 2000 °C in vacuum or inert atmosphere, and have the characteristics of low density, radiation protection, ablation resistance, high specific strength and specific modulus, it sets standards for high-performance ultra-high temperature thermal insulation material [8–13]. In the early stage, we prepared C/C-SiCO nanoporous ceramic composites by repeatedly impregnating C/CA with SiCO precursor [14]. On the one hand, it can improve the high-temperature thermal insulation performance of SiCO ceramics. On the other hand, the three-dimensional network framework of carbon aerogel can be used to shape carbon fibres, thus improving the ability of carbon fibres to resist shrinkage. However, the high-temperature oxidation resistance and ablation resistance of C/C-SiCO nanoporous ceramic composites still need further improvement.

In addition, coating method, as a widely used surface modification technology, can prolong the service life of materials and improve their reliability in complex environments. The coating preparation methods include slurry method [15,16], embedding method [17], plasma spraying method [18,19], chemical vapour deposition (CVD) method [20], etc. According to the raw material composition, the coating can be divided into glass, ceramic, composite coating, etc. [21–23]. Du *et al.* [24] prepared MoSi₂-SiC_w-SiB₆-borosilicate glass/TaSi₂-MoSi₂-SiC_w-SiB₆-borosilicate glass composite coatings on the surface of CBCF composite materials through rapid sintering method, and evaluated the oxidation resistance of the coatings from room temperature to 1527 °C in an arc tunnel. Xu *et al.* [25] prepared a ZrB₂-SiC_w-borosilicate glass/ZrB₂-MoSi₂-SiC_w-borosilicate glass composite coating. The weight loss rate of the material was only 0.44% after oxidation at 1500 °C for 100 min. The coating can effectively protect the substrates from high-temperature corrosion.

In our earlier work [26], a TaSi₂-MoSi₂-ZrB₂-borosilicate glass coating was prepared on the surface of porous carbon fibre-reinforced SiCO ceramic composites (C-SiCO), and the anti-oxidation properties and ablation resistance for 90 s of coated sample were investigated. In this paper, the effects of SiCO precursors on the ablation resistance of C/C-SiCO nanoporous ceramic composites were investigated. Furthermore, TaSi₂-MoSi₂-borosilicate glass coatings or

TaSi₂-MoSi₂-ZrB₂-borosilicate glass coatings were prepared on the C/C-SiCO surface to improve its performance. The effects of coating composition and thickness on the ablation resistance for 200 s of the integrated materials were studied.

II. Experimental

2.1. Materials

Methyltrimethoxysilane (MTMS) and dimethyldiethoxysilane (DMDDES) were purchased from Wuhan Yi Hua Cheng Technology Development Co. (China). Ethanol and nitric acid came from China National Pharmaceutical Group Co. Ltd. TaSi₂, MoSi₂, ZrB₂, Al₂O₃, B₂O₃ and SiO₂ were purchased from Sinopharm Chemical Reagent Co. (China). Deionized water was self-made. Analytical pure chemicals were used and they were not further processed before use.

2.2. Preparation of C/C-SiCO ceramic composites

In the first step, the SiCO precursor sol was prepared as follows: methyltrimethoxysilane (MTMS) and dimethyldiethoxysilane (DMDDES) were well mixed with a certain amount of ethanol solution (EtOH) and deionized water (H₂O). Then, 0.1 mol/l nitric acid (HNO₃) was added to this mixed solution and the solution was kept stationary for 3–5 h after stirring for 30 min. In the obtained solution a certain amount of mixed solution of EtOH and ammonia hydroxide (NH₃ · H₂O) was slowly added and stirred evenly for 15–20 min to make them sufficiently polymerized under alkaline conditions. This enabled formation of final SiCO precursor sol with the molar ratio of MTMS/DMDDES/H₂O/EtOH/HNO₃/NH₃ · H₂O = 0.844 : 0.236 : 2.833 : 0.855 : 0.001 : 0.032.

In the second step, the carbon aerogel composites (C/CAs) were fabricated by impregnation of polyacrylonitrile-based carbon fibre porous structure with RF sol and subsequent supercritical drying and pyrolysis at high temperatures (i.e. 1200 and 1600 °C) were performed (Fig. 1). The obtained porous C/CAs were then impregnated with the pre-prepared SiCO precursor sol under a vacuum and the C/CA sample containing SiCO was sealed in a 65 °C water bath for 3 days and fully aged. Next, the cured C/CA-SiCO aqua gel composites were soaked in ethanol for 3 days, with ethanol exchanging once each day. After that, it was

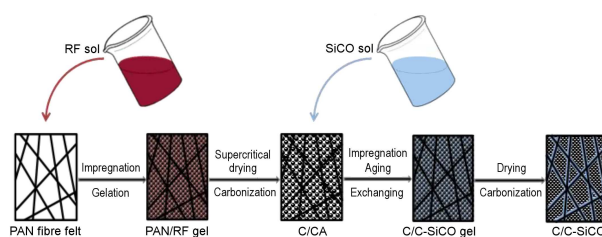


Figure 1. Schematic illustration of the synthesis process of C/C-SiCO

Table 1. Compositions of TaSi₂-MoSi₂ based coatings

		MoSi ₂ [wt.%]	TaSi ₂ [wt.%]	SiB ₆ [wt.%]	Borosilicate glass [wt.%]	ZrB ₂ [wt.%]
TM-BG coating	Outer coating	48	30	2	20	0
	Inner coating	58	0	2	40	0
TMZ-BG coating	Outer coating	40	25	2	28	5
	Inner coating	45	0	2	48	5

heated and dried in air at 50, 80 and 100 °C for 1 day each. Finally, C/C-SiCO nanoporous ceramic composites were obtained by CO₂ supercritical drying and pyrolysis in nitrogen atmosphere at 1200 °C (Fig. 1). The obtained samples were denoted as [C/C-SiCO]-1. The above vacuum impregnation until the pyrolysis process was repeated once and twice to obtain ceramic composites named [C/C-SiCO]-2 and [C/C-SiCO]-3, respectively.

2.3. Preparation of coatings

The obtained C/C-SiCO composites with a size of 15 mm × 15 mm × 15 mm were used as substrates after hand-polishing, chamfering and drying in an oven at 100 °C. TaSi₂-MoSi₂-borosilicate (TM-BG coating) and TaSi₂-MoSi₂-ZrB₂-borosilicate (TMZ-BG coating) glass coatings were prepared on the surfaces of substrates by slurry-sintering method.

The preparation started with thoroughly mixing 5 wt.% Al₂O₃, 15 wt.% B₂O₃ and 80 wt.% SiO₂ powders in a ball mill and which were sieved and placed in a muffle furnace. The muffle furnace was heated to 1500 °C at a rate of 10 °C/min and kept for 1.5 h. After cooling in the furnace, the obtained glass block was ground into glass powder and the powder was then sieved using a 300-mesh screen. According to the compositions given in Table 1, the raw coating powder was mixed with ethanol solution and placed in a ball milling tank. The grinding ball : mixed powder : ethanol volume ratio was 2 : 1 : 3, and the coating slurry with particle size of 1–10 μm was obtained by ball milling at a speed of 220 r/min for 24 h. Then, the coating slurry was uniformly deposited on the substrate surface by brushing and the ethanol solution was evaporated in an oven at 100 °C in a timely manner. The gradient coating with different thickness was prepared by repeating the steps of brushing and drying for several times. Thus, the samples with set of 4 layers of inner and outer coatings were obtained by brushing with total number of cycles corresponding to 8, 16 and 24. Finally, the C/C-SiCO with coating was prepared using graphite powder embedded sintering process in an air atmosphere with sintering time of 30 min and sintering temperature of 1315 °C.

2.4. Characterization

High-temperature stability of the samples was carried out in a muffle furnace (KBF700, Lab, China) for 1–60 min. The weight loss rate and thickness shrinkage rate of the samples were calculated by measuring the weights and dimensions before and after heat treatment in air at 1600 °C. The DR6130 ablation instrument

Table 2. Oxyacetylene flame ablation process parameters

Gas	Flow [l/h]	Purity [%]
O ₂	1000	>98
C ₂ H ₂	400	>99.2

was used to evaluate the ablation resistance and a dual-colorimetric infrared thermometer to record the real-time temperature of the cold surface (non-ablated surface) of the sample. The sample was placed in a graphite mould and fixed on the ablation instrument. The nozzle diameter was 2 mm and the nozzle was positioned 35 mm away from the sample. The ablation process parameters were adjusted according to Table 2. The ablation resistances of the sample based on the mass ablation rate R_m (g/s) and linear ablation rate R_d (mm/s) were calculated from the following equations:

$$R_m = \frac{m_0 - m_1}{t} \quad (1)$$

$$R_d = \frac{d_0 - d_1}{t} \quad (2)$$

where m_0 and m_1 are the masses of the ablation sample before and after the test, d_0 and d_1 are the thickness of the central area of the ablation sample before and after the test and t is the ablation time.

Phase composition of the samples was analysed by German Bruker Model D8 Advance X-ray diffractometer (using Cu K α radiation in 2 θ range from 10° to 80°). The microstructure of the sample was observed using a Japanese S-4800 field emission scanning electron microscope. Platinum was sputtered for 45 s before the test and the test voltage was 1–15 kV. Energy dispersive spectroscopy (EDS) analyser was simultaneously used to scan and analyse the local elemental composition and content of the sample.

III. Results and discussion

3.1. High-temperature stability

Figure 2 shows the thermal stability of the C/CA and C/C-SiCO nanoporous ceramic composites after heat treatment at 1600 °C for different times. It can be seen that as the number of impregnation/pyrolysis steps increases, both the weight loss and thickness shrinkage of the C/C-SiCO continue to decrease after the same heat treatment time, and are much smaller than that of the C/CA after heat treatment under the same conditions. After heat treatment in air atmosphere at 1600 °C for 1 min, the C/CA sample showed weight loss of 26.8%, while the weight losses of the C/C-SiCO sam-

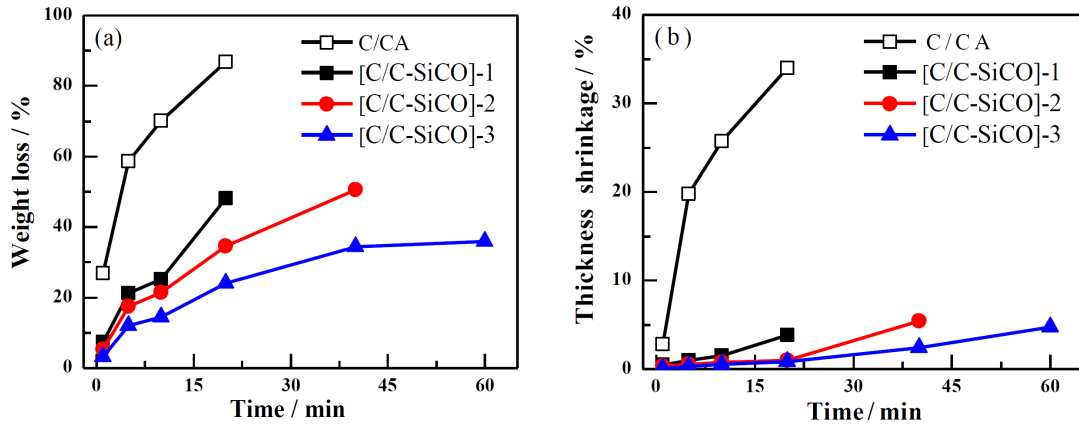


Figure 2. Weight loss (a) and thickness shrinkage (b) of C/CA and C/C-SiCO after heat treatment in air at 1600 °C for different time

ples impregnated/pyrolysed 1, 2 and 3 times were 7.3%, 5.3% and 3.2%, respectively. This indicates that repeated impregnation/pyrolysis steps can effectively improve the high-temperature resistance of the C/CA in air atmosphere. In addition, under conditions of equivalent weight loss, the [C/C-SiCO]-3 can withstand the longest heat treatment time (with a weight loss of 35.9% after 60 min of heat treatment). In summary, increasing the number of impregnation/pyrolysis steps of the SiCO precursor sol gives improved high-temperature stability of the C/C-SiCO nanoporous ceramic composites to some extent.

3.2. Ablation resistance

Figures 3a and 3b show photos of the C/C-SiCO nanoporous ceramic composites before and after acetylene flame ablation test at 1600 °C for 200s, respectively. It can be observed that the ablation zone of the [C/C-SiCO]-1 has pits, while the ablation surfaces of

the [C/C-SiCO]-2 and [C/C-SiCO]-3 samples remain flat (no defects such as peel off or delamination have appeared). After ablation, white matter also precipitated from the edge of the sample surface and spread along the thickness direction. As the number of impregnation/pyrolysis steps increased, the white phase area decreased and the sample morphology remained less damaged.

After ablation by an oxygen acetylene flame at 1600 °C for 200s, the ablation rate of the C/C-SiCO with different pyrolysis temperatures of the C/CA is shown in Figures 3c and 3d. It can be seen that with the increase of the number of impregnation/pyrolysis steps, the mass and linear ablation rates of the C/C-SiCO continue to decrease. In addition, the C/C-SiCO has better ablation resistance when the C/CA pyrolysis temperature was 1200 °C. The sample mass ablation rates of the C/C-SiCO samples impregnated/pyrolysed 1, 2 and 3 times were 0.0011, 0.0007 and 0.0005 g/s, respectively

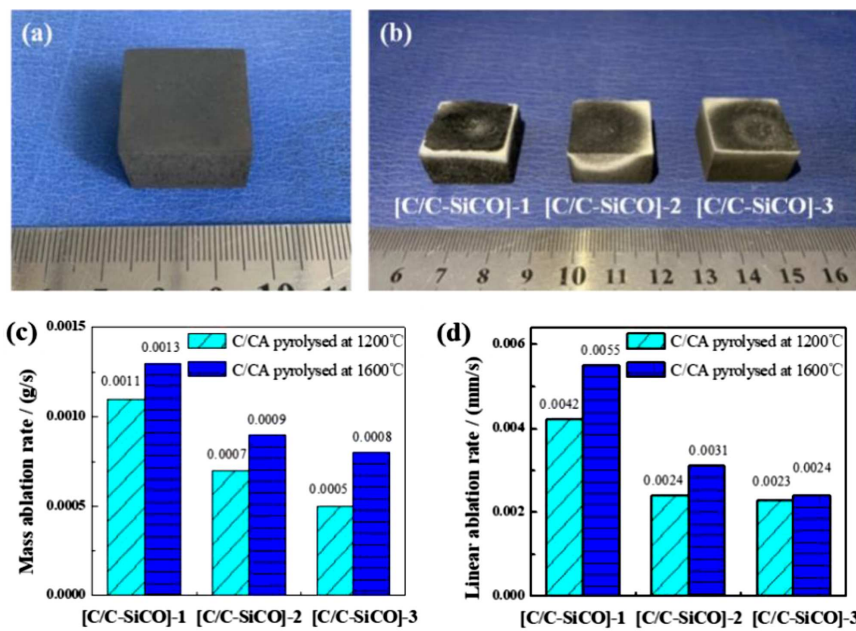


Figure 3. Photographs of C/C-SiCO before (a) and after (b) ablation and mass (c) and linear ablation rate (d) of C/C-SiCO prepared by using different pyrolysis temperatures of C/CA

(decreased by 36% and 29%). The viscous flow state SiO₂ formed by the oxidation of SiCO ceramic matrix at 1600 °C can form an oxygen barrier layer on the surface of the C/C-SiCO. Repeated impregnation and pyrolysis can make the SiO₂ layer more complete and effectively prevent oxygen from invading the interior of the C/C-SiCO. The C/C-SiCO is mainly open-pore structure, with closed pores in the matrix. During the ablation process, the sample will be partially eroded due to the existence of open pores, while the closed pores continue to expand at high temperatures. When the maximum pressure that the pore wall can withstand is exceeded, the composites will be destroyed. Compared with the C/CA pyrolysis at 1200 °C, the C/C-SiCO prepared by C/CA pyrolysed at 1600 °C has a slightly lower density and contains slightly more pores per unit volume, resulting in a higher ablation rate. In conclusion, reducing the pyrolysis temperature of the C/CA or increasing the number of impregnation/pyrolysis steps of the SiCO precursor sol can enhance the ablation resistance of C/C-SiCO nanoporous ceramic composites to a certain extent.

3.3. Effect of coatings on ablation resistance

It was shown (Fig. 3) that the ablation resistance of the C/C-SiCO ceramic composites was significantly improved when the number of impregnation/pyrolysis steps was increased from 1 to 2. However, there is little difference in the ablation rate between the [C/C-SiCO]-2 and [C/C-SiCO]-3 composites. At the same time, considering that increasing the number of impregnation/pyrolysis steps will increase the density of the C/C-SiCO and reduce its thermal insulation performance, the [C/C-SiCO]-2 sample was selected as the substrate material, and TM-BG coating or TMZ-BG coating were prepared on its surface. In this work, the samples with set of 4 layers of inner and outer coatings were obtained by brushing with total number of cycles corresponding to 8, 16 and 24. After each deposition, the ethanol solution was evaporated in a 100 °C drying oven before proceeding with the next application. Figure 4 shows photographs of the TM-BG and TMZ-BG coated samples. The surface of the coating is smooth without defects (such as flaking, blistering, cracking, etc.) and the shape of the coated sample remains unchanged after sintering.

Figures 5a and 5d show photographs of the TM-BG and TMZ-BG coated samples after being ablated by an oxygen acetylene flame at 1600 °C for 200 s, respectively. It can be seen that the coating is intact and does not peel off after ablation, without macroscopic cracks, ablating pits and other defects. The sample size is unchanged and both coatings can provide good protection for the substrates. Figures 5b and 5c show ablation rate of the TM-BG coated sample after ablation at 1600 °C for 200 s. It can be seen that with the increase of brushing cycles, both mass ablation rate and linear ablation

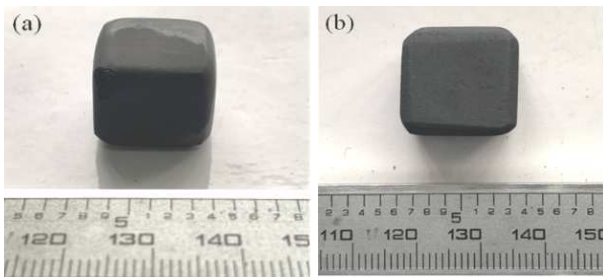


Figure 4. Photographs of the TM-BG (a) and the TMZ-BG (b) coated samples

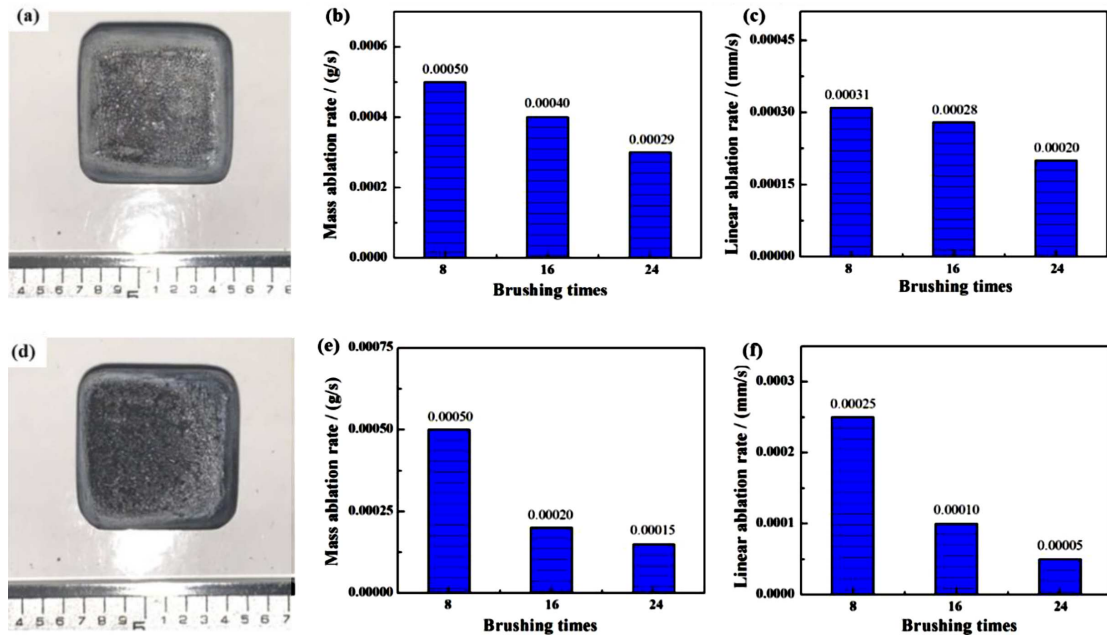


Figure 5. Photographs of TM-BG (a) and TMZ-BG (d) coated [C/C-SiCO]-2 samples after ablation; mass (b) and linear (c) ablation rates of the TM-BG coated sample with different brushing cycles; mass (e) and linear (f) ablation rates of the TMZ-BG coated sample with different brushing cycles

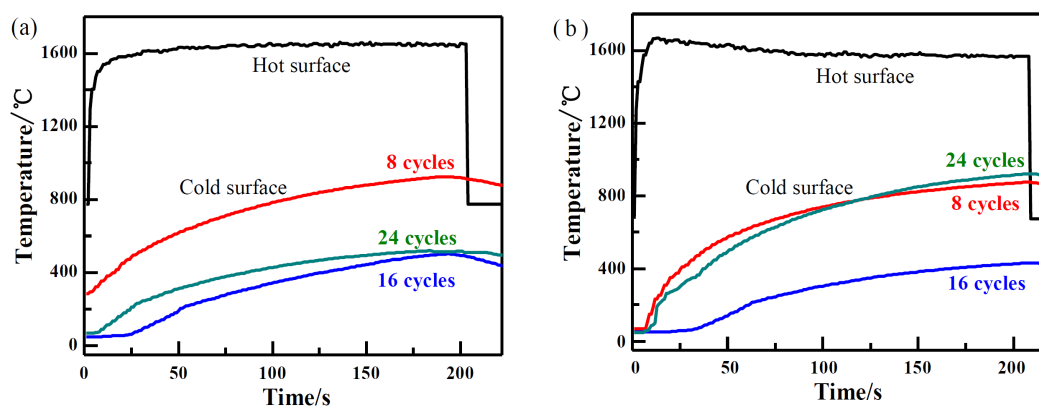


Figure 6. Change of surface temperature during ablation of: a) TM-BG and b) TMZ-BG coated [C/C-SiCO]-2 samples

rate of the coated sample continue to decrease, indicating that increasing the coating thickness is beneficial for enhancing the ablation resistance of the sample. The ablation resistance of the sample is not only affected by the thermal expansion matching between the coating and the substrates at high temperatures, but also by the ablation degree of the sample by the oxygen acetylene flame in the test. Under the same ablation conditions, the thicker the coating, the better the protection of the substrates. Figures 5e and 5f show ablation rates of the TMZ-BG coated sample after ablation at 1600 °C for 200 s. Similarly, as the brushing number increases, the mass ablation rate and linear ablation rate of the sample gradually decrease. In addition, the mass ablation rate and linear ablation rate of the TMZ-BG coated sample are lower than that of the TM-BG coated sample, indicating that the TMZ-BG coating is more stable under 1600 °C oxygen acetylene flame ablation, and the C/C-SiCO with TMZ-BG coating has better ablation resistance.

According to the results described in section 3.2, after being ablated by an oxygen acetylene flame at 1600 °C for 200 s, the mass ablation rate and linear ablation rate of the [C/C-SiCO]-2 sample were 7×10^{-4} g/s and 2.4×10^{-3} mm/s, respectively. Under the same conditions, the mass ablation rate and linear ablation rate of the [C/C-SiCO]-2 modified by TM-BG coating (24 cycles of brushing) decreased by 59% and 92%, and that

modified by TMZ-BG coating decreased by 79% and 99%, respectively. Thus, it was proved that the coating significantly enhanced the ablation resistance of the C/C-SiCO ceramic composites.

The surface temperature curves of the TM-BG and TMZ-BG coated [C/C-SiCO]-2 samples during oxygen-acetylene flame ablation at 1600 °C/200 s are shown in Fig. 6. It can be seen that the coated sample with 16 cycles of brushing had the lowest temperature on the cold surface (non-ablative surface). Because the thickness of the sintered coating is moderate at this time, under the ablation of high-temperature oxygen acetylene flame, the coating can not only use its high emissivity to dissipate a large amount of heat from the surface, but also can better protect the substrates from being damaged and effectively plays its heat insulation advantage. When the number of brushing cycles is 16, the maximal cold surface temperatures of the TM-BG and TMZ-BG coated samples after the ablation are 496 and 429 °C, respectively. Combined with the ablation rate calculated in the previous paper, it can be proved that the TMZ-BG coating has better ablation resistance performance.

XRD was used to analyse the phase composition of the coating surface after ablation at 1600 °C for 200 s. It can be seen (Fig. 7a) that there are MoSi_2 , Mo_5Si_3 , SiO_2 , Ta_2O_5 and TaO phases in the TM-BG coating after ablation. The content of MoSi_2 in the raw material component is relatively high. At lower temperatures, MoSi_2

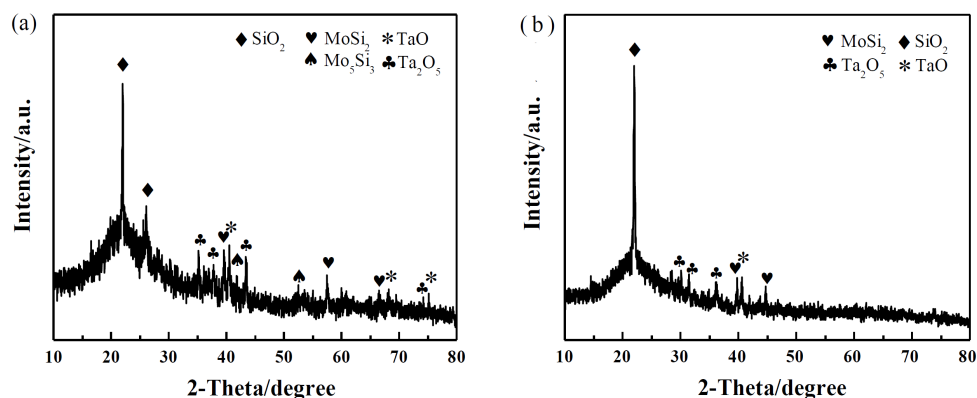
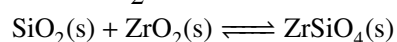
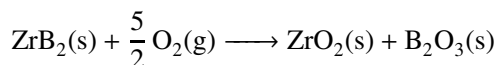
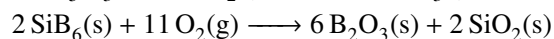
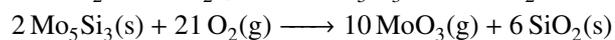
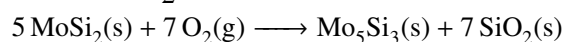
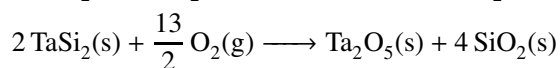
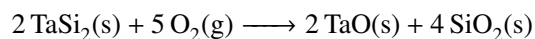


Figure 7. XRD patterns of: a) TM-BG and b) TMZ-BG coating samples after ablation

undergoes complete oxidation to generate MoO_3 and clustered SiO_2 , forming a loose structure that accelerates the diffusion of oxygen in the coating. MoSi_2 undergoes selective oxidation at higher temperature [27], and the generated Mo_5Si_3 is further oxidized to form gaseous MoO_3 . The volatilization of MoO_3 forms pores in the coating, while a dense SiO_2 oxide film continuously forms on the surface of the coating. TaSi_2 generates Ta_2O_5 or TaO under different oxygen partial pressure, while MoSi_2 , TaSi_2 and SiB_6 generate SiO_2 after oxidation [28,29], so the crystalline characteristic peak of SiO_2 in XRD pattern is strong. As it can be seen from Fig. 7b, compared with the XRD pattern of TM-BG coating, TaO phase on the surface of the TMZ-BG coating disappears after ablation, and TaSi_2 is completely oxidized into Ta_2O_5 phase with better oxidation resistance. Due to the small content of ZrB_2 in the coating raw material, no phase containing Zr element was detected after ablation. In addition, the broad peak appearing at about $2\theta = 23^\circ$ in the XRD pattern is the amorphous peak of glass, which shows that the borosilicate glass in the coating after ablation is still amorphous. Borosilicate glass exhibits a viscous flow state at high temperatures in an oxygen acetylene flame, which can timely bridge the pores and cracks formed on the coating surface by high-speed airflow, bond other components of the coating, so as to display a better ablative resistance. In summary, the coating mainly undergoes the following chemical reactions and produces different oxidation products under different oxygen partial pressures [30].



Figures 8a-c show the surface microstructures of the TM-BG coated sample after being ablated by an oxygen acetylene flame at 1600°C for 200 s. It can be seen that the edge region of the ablated coating surface is dense and unchanged. According to the above XRD analysis, it is believed that SiO_2 glass in a viscous flow state forms an oxide film. However, the coating at the ablation centre exhibits peeling phenomenon, with particles of different sizes stacked together and a small amount of micro lines appearing. The surface of the coating is covered with discontinuous glass phases, as observed in Fig. 8c. This is because part of the glass phase is washed away or gradually volatilized by a high-temperature oxygen acetylene flame, resulting in crystal particles with different morphologies formed by other components exposed on the coating surface after cooling. Based on the XRD analysis (Fig. 7a), it can be seen that the blocky particles are Mo_5Si_3 and Ta_2O_5 that have not been completely oxidized.

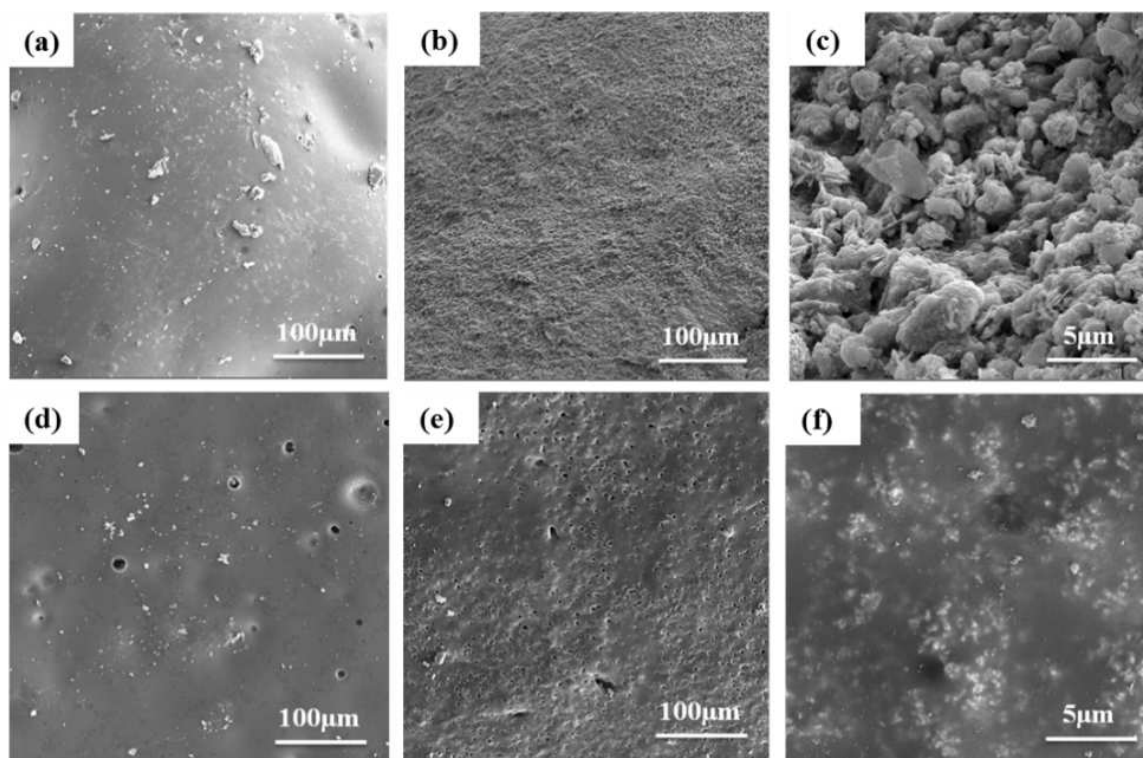


Figure 8. Surface SEM images of TM-BG coating (a-c) and TMZ-BG coating (d-f) samples after ablation - edge (a,d) and centre (b,c,e,f)

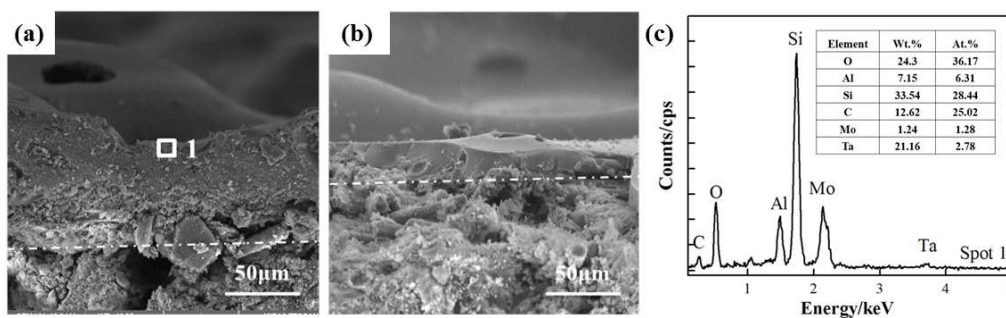


Figure 9. Cross-sectional SEM images of: a) TM-BG and b) TMZ-BG coatings after ablation and c) EDS analysis at point 1

Figures 8d-f show the surface microstructures of the TMZ-BG coating sample after ablation at 1600 °C for 200 s. It can be observed that the edge region of the ablated surface is covered by a grey dense layer, with a small number of depressions and bubble-like pores, as well as white particles of varying sizes. From the previous analysis, it can be seen that the occurrence of “depressions” is due to the volatilization of borosilicate glass with lower viscosity during ablation. The formation of pores is not only related to the volatilization of glass, but also may be caused by the overflow of some gaseous oxidation products from the coating surface at high temperatures. The grey dense layer is the SiO₂ glass oxide layer. During the ablation process, in addition to the SiO₂ in the borosilicate glass, the SiO₂ produced by the oxidation of silicides from the coating components also presents a viscous flow state at 1600 °C, and the holes and micro-cracks on the coating surface are constantly healed. However, there are many small circular holes in the ablation centre of the sample, which is because the central area is more seriously scoured by oxygen acetylene flames. The SiO₂ on the coating surface fails to self-heal the defects in a timely manner during the ablation process, resulting in small pores left on the coating surface after cooling. The ablation centre remains smooth and dense, with some white particles embedded in the glass phase. Compared with the TM-BG coating after ablation (Fig. 8c), there was no obvious peeling phenomenon in the centre of the TMZ-BG coating after ablation, indicating that its ablation resistance is better than that of the TM-BG coating.

Figure 9 shows the microstructure and EDS of the ablation centre section of the TM-BG and TMZ-BG coated samples after ablation at 1600 °C for 200 s. It can be seen that although the surface of the coating is uneven, there are no through-holes formed in the thickness direction, and the coating tightly covers the surface of the substrates without any layering or peeling. In addition, the TMZ-BG coating is denser than the TM-BG coating, indicating that the addition of ZrB₂ has a certain contribution to improving the ablation resistance of the coating. EDS analysis at point 1 (Fig. 9c) confirmed that the coating surface is composed of oxidation products of TaSi₂ and MoSi₂ embedded in the viscous-state SiO₂ glass oxide layer. At high temperature, the viscous glass phase covers the surface of the coating, thereby

covering the surface defects. At the same time, the penetration rate of oxygen in SiO₂ is extremely low. The SiO₂ oxide layer on the coating surface and the SiO₂ layer in the substrates provide dual protection for the C/C-SiCO nanoporous ceramic composites. The C/C-SiCO modified by coating exhibits good ablation resistance under the ablation of oxygen acetylene flame.

IV. Conclusions

C/C-SiCO nanoporous ceramic composites were prepared by repeated impregnation and pyrolysis of SiCO precursor sol. After that TM-BG or TMZ-BG coatings on the C/C-SiCO surfaces were obtained by slurry brushing combined with graphite powder embedding sintering process. As the number of impregnation/pyrolysis steps of SiCO precursor sol increases, the ablation rates of the C/C-SiCO at 1600 °C for 200 s decrease continuously. Repeated impregnation and pyrolysis make the SiCO precursors more filled in the C/C-SiCO matrix, and the SiO₂ layer formed by oxidation at high temperatures is more complete, thus providing more effective protection for the C/C-SiCO.

After ablation at 1600 °C for 200 s, both the TM-BG and TMZ-BG coatings are intact and does not peel off. The sample sizes remain unchanged and the ablation rate is significantly reduced compared with that of the uncoated C/C-SiCO. Coating modification can significantly enhance the ablation resistance of the C/C-SiCO. The ablation resistance of the coated sample increases with the increase of the number of brushing cycles. The TMZ-BG coated samples are more stable under oxygen acetylene flame ablation.

Acknowledgements: Authors would like to thank Eceshi (www.eceshi.com) for the SEM analysis and Shiyanjia Lab (www.shiyanjia.com) for the XRD measurements.

References

1. W. Huang, H. Qin, S. Luo, Z. Wang, “Research status of key techniques for shock-induced combustion ramjet (shcramjet) engine”, *Sci. China Ser. E*, **53** [1] (2010) 220–226.
2. D.A. Stewart, D.B. Leiser, “Lightweight TUFROC TPS for hypersonic vehicles”, *AIAA 2006-7945*, 2006.

3. L. Qiu, Y.M. Li, X.H. Zheng, J. Zhu, D.W. Tang, J.Q. Wu, C.H. Xu, “Thermal-conductivity studies of macro-porous polymer-derived SiOC ceramics”, *Int. J. Thermophys.*, **35** [1] (2014) 76–89.
4. T. Varga, A. Navrotsky, J.L. Moats, R.M. Morcos, F. Poli, K. Müller, A. Sahay, R. Raj, “Thermodynamically stable $\text{Si}_x\text{O}_y\text{C}_z$ polymer-like amorphous ceramics”, *J. Am. Ceram. Soc.*, **90** [10] (2007) 3213–3219.
5. P.N. Adler, “Overview of ARPA low-cost ceramic composites (LC3) program”, *Proceedings of the 41st International SAMPE Symposium and Exhibition*, Part 1, (1996) 524–531.
6. N. Zhao, J. Feng, Y. Jiang, J. Feng, “Preparation and characterization of Si-C-O aerogel composites for thermal insulation”, *J. Chin. Ceram. Soc.*, **40** [10] (2012) 1473–1477.
7. X. Li, J. Feng, Y. Jiang, L. Li, J. Feng, “Preparation and properties of PAN based carbon fiber reinforced SiCO aerogel composites”, *Ceram. Int.*, **45** [14] (2019) 17064–17072.
8. J. Feng, J. Feng, Y. Jiang, C. Zhang, “Ultralow density carbon aerogels with low thermal conductivity up to 2000 °C”, *Mater. Lett.*, **65** [23–24] (2011) 3454–3456.
9. J. Feng, C. Zhang, J. Feng, “Carbon fiber reinforced carbon aerogel composites for thermal insulation prepared by soft reinforcement”, *Mater. Lett.*, **67** [1] (2012) 266–268.
10. L. Wang, J. Feng, S. Zhang, Q. Sun, Y. Luo, “Dual-channel coextrusion printing strategy towards mechanically enhanced, flame retardant, and thermally stable polyimide-silica aerogels for thermal insulation”, *Addit. Manuf.*, **71** (2023) 103583.
11. W. Ding, H. Li, H. Liu, Y. Zheng, “Thermal insulation and antioxidation of vertical graphene oxide-grafted carbon nanofiber aerogels with ceramic coating”, *J. Am. Ceram. Soc.*, **106** [4] (2023) 2501–2514.
12. L. Li, J. Feng, F. Liu, L. Li, Y. Jiang, J. Feng, “Mechanical and thermal insulation properties of carbon fibre-reinforced carbon aerogel composites”, *Adv. Appl. Ceram.*, **121** [5–8] (2022) 222–230.
13. F. Liu, Y. Jiang, J. Feng, L. Li, J. Feng, “Dual template strategy to prepare ultralight and high-temperature resistant ceramic nanorod aerogels for efficient thermal insulation”, *Ceram. Int.*, **49** [14] (2023) 22677–22689.
14. X. Li, J. Feng, Y. Jiang, L. Li, J. Feng, “Anti-oxidation performance of carbon aerogel composites with SiCO ceramic inner coating”, *Ceram. Int.*, **45** [8] (2019) 9704–9711.
15. V.V. Rodionova, G.A. Kravetkii, N.M. Schestakova, A.V. Kuznetsov, V.I. Kostikov, A.V. Demin, “Anti-oxidation protection of carbon-based materials”, *US Patent* 5660880, 1997.
16. N. Zhu, Y. Hou, W. Yang, C. Zhong, L. Zhang, D. Wang, R. Zhang, L. Li, G. Wen, “Additive manufacturing low shrinkage Si-based composite ceramics with SiCO microsphere/polyvinyl silicon acetylene slurry”, *J. Eur. Ceram. Soc.*, **42** [15] (2022) 6925–6934.
17. Q.G. Fu, H.J. Li, X.H. Shi, K.Z. Li, G.D. Sun, “Silicon carbide coating to protect carbon/carbon composites against oxidation”, *Scripta Mater.*, **52** [9] (2005) 923–927.
18. M. Huang, K. Li, H. Li, Q. Fu, G. Xu, G. Sun, “Investigation on microstructure and oxidation resistance of Cr-Al-Si coating for carbon/carbon composites by plasma spraying”, *Acta Materialiae Compositae Sinica*, **24** [5] (2007) 109–112.
19. A. Dobrádi, M.E. Bódogh, K. Kovács, “Plasma spraying of bioactive glass-ceramics containing bovine bone”, *Process. Appl. Ceram.*, **11** [2] (2017) 113–119.
20. Y.C. Zhu, S. Ohtani, Y. Sato, N. Iwamoto, “The improvement in oxidation resistance of CVD-SiC coated C/C composites by silicon infiltration pretreatment”, *Carbon*, **36** [7–8] (1998) 929–935.
21. D.A. Berztiss, R.R. Cerchiara, E.A. Gulbransen, F.S. Pettit, G.H. Meier, “Oxidation of MoSi_2 and comparison with other silicide materials”, *Mater. Sci. Eng. A*, **155** [1–2] (1992) 165–181.
22. A. Nyczyk-Malinowska, W. Niemiec, G. Smola, R. Gawel, M. Szuwarzynski, Z. Grzesik, “Preparation and characterization of oxidation-resistant black glass (SiCO) coatings obtained by hydrosilylation of polysiloxanes”, *Surf. Coat. Technol.*, **407** (2021) 126760.
23. S. He, X. Wu, X. Zhang, J. Sun, F. Tian, S. Guo, H. Du, P. Li, Y. Huang, “Preparation and properties of thermal insulation coating based on silica aerogel”, *Energ. Buildings*, **298** (2023) 113556.
24. B. Du, C. Hong, S. Zhou, C. Liu, X. Zhang, “Multi-composition coating for oxidation protection of modified carbon-bonded carbon fiber composites”, *J. Eur. Ceram. Soc.*, **36** [14] (2016) 3303–3310.
25. B. Xu, C. Hong, Q. Qu, X. Zhang, J. Han, N. Li, K. Gui, G. Zhao, C. Liu, “Preparation of a multi-composition coating for oxidation protection of modified carbon-bonded carbon fiber composites by a rapid sintering method”, *Surf. Coat. Technol.*, **270** (2015) 109–116.
26. X. Li, J. Feng, Y. Jiang, H. Lin, J. Feng, “Preparation and properties of TaSi_2 - MoSi_2 - ZrO_2 -borosilicate glass coating on porous SiCO ceramic composites for thermal protection”, *Ceram. Int.*, **44** [16] (2018) 19143–19150.
27. P.J. Meschter, “Low-temperature oxidation of molybdenum disilicide”, *Metall. Mater. Trans. A*, **23** [6] (1992) 1763–1772.
28. G. Shao, X. Wu, Y. Kong, X. Shen, S. Cui, X. Guan, C. Jiao, J. Jiao, “Microstructure, radiative property and thermal shock behavior of TaSi_2 - SiO_2 -borosilicate glass coating for fibrous ZrO_2 ceramic insulation”, *J. Alloys Compd.*, **663** (2016) 360–370.
29. X. Tao, X. Li, L. Guo, X. Xu, A. Guo, F. Hou, J. Liu, “Effect of TaSi_2 content on the structure and properties of TaSi_2 - MoSi_2 -borosilicate glass coating on fibrous insulations for enhanced surficial thermal radiation”, *Surf. Coat. Technol.*, **316** (2017) 122–130.
30. X. Yong, L. Cao, J. Huang, W. Kong, J. Su, C. Li, H. Ouyang, L. Zhou, J. Liu, “Microstructure and oxidation protection of a $\text{MoSi}_2/\text{SiO}_2$ - B_2O_3 - Al_2O_3 coating for SiC-coated carbon/carbon composites”, *Surf. Coat. Technol.*, **311** (2017) 63–69.